Cellular/Molecular

Collaboration of PSD-Zip70 with Its Binding Partner, SPAR, in Dendritic Spine Maturity

Hisato Maruoka, Daijiro Konno, Kei Hori, and Kenji Sobue
Department of Neuroscience, Osaka University Graduate School of Medicine, Suita City, Osaka 565-0871, Japan

Recent studies have reported on the molecular mechanisms underlying dendritic spine (spine) dynamics. Because most of these studies investigated spine dynamics by overexpressing constitutively active or dominant-negative PSD (postsynaptic density) proteins in cultured mature neurons, the results represent the enlargement of mature spines or their return to an immature state. Here, we developed the technique of *in utero* electroporation to investigate spine dynamics. Using this technique, we demonstrated the suppression of spine maturation by the C-terminal variants of PSD-Zip70 *in vitro* and *in vivo*. Transient overexpression of the C terminus of PSD-Zip70 and knock-down of PSD-Zip70 also displayed the destabilization of mature spines. We further found the PSD-Zip70 and SPAR (spine-associated RapGAP) interaction via the short C-terminal region of PSD-Zip70 and the GK-binding domain of SPAR. In association with immature spines induced by overexpression of the PSD-Zip70 C terminus or knock-down of PSD-Zip70, SPAR lost its spine localization. Overexpression of the GK-binding domain of SPAR also induced to form immature spines without affecting the localization of PSD-Zip70 in the small heads of filopodial spines. Our results suggest that PSD-Zip70 in collaboration with SPAR is critically involved in spine maturity, especially in the mature spine formation and the maintenance of spine maturity.

Key words: **dendritic spine; postsynaptic density; *in utero* electroporation; spine dynamics; filopodia; knock-down**

Introduction

Recent imaging studies have revealed an instructive role of dendritic spines (spines) in synaptic plasticity. During synaptogenesis, dendrites have a high density of filopodia, which exhibit protrusive activity on a timescale of minutes (Jontes and Smith, 2000; Segal, 2001; Bonhoeffer and Yuste, 2002; Goda and Davis, 2003). Some filopodia contact nearby axons to form synapses and mature into mushroom-shaped short spines as a postsynaptic structure. After the completion of synaptic formation, the spines are still dynamic in response to excitatory synaptic input. One of the main molecular bases for such dynamics is the actin cytoskeleton (Matus, 2000). Fischer et al. (1998) studied spine dynamics using cultured neurons expressing GFP (green fluorescent protein)-tagged actin and found that the actin polymerization/depolymerization equilibrium reflects the spine dynamics. Accumulating evidence suggests the involvement of actin regulators, such as small GTPases (Tashiro et al., 2000), cortactin (Hering and Shen, 2003), catenins (Murase et al., 2002; Abe et al., 2004), and drebrin (Hayashi and Shirao, 1999), in spine dynamics. The electron-dense structure of excitatory synapses known as the PSD (postsynaptic density), which underlies the postsynaptic membrane of the spine head, is the center for controlling spine dynamics. Organization of the PSD involves glutamate receptors, cytoskeletal elements as described above, signaling molecules, and PSD scaffold proteins (Sheng and Kim, 2002; Ehlers, 2003; McGee and Bredt, 2003). Indeed, the overexpression of PSD-95 (El-Husseini et al., 2000), Shank and Homer family members (Carlo et al., 2001), Kalirin (Penzes et al., 2001, 2003), SPAR (spine-associated RapGAP) (Pak et al., 2001), and Eph receptors (Irie and Yamaguchi, 2002; Murai et al., 2003) and their mutants cause changes in the shape, size, and number of spines. Despite these numerous findings, the molecular mechanisms underlying spine dynamics are not fully understood.

To study the molecular organization and function of the PSD, we cloned numerous hybridoma cell lines that produced monoclonal antibodies (mAbs) against PSD preparations. Using one of these mAbs, we isolated an EVH-1 (Ena/VASP homology domain 1) domain and a unique leucine-zipper motif-containing PSD scaffold protein, PSD-Zip45 (Homer 1c) (Sun et al., 1998; Tadokoro et al., 1999), and demonstrated the dynamic turnover and compartmentalization of this protein within spines (Okabe et al., 2001; Usui et al., 2003). We also isolated a novel PSD protein, PSD-Zip70, which has a consensus sequence for N-terminal myristoylation and polybasic cluster in its N terminus, and three leucine-zipper motifs, a coiled-coil domain, and a PDZ-binding sequence in its C terminus (Tachibana et al., 1999; Konno et al., 2002). A human homolog of PSD-Zip70 was independently reported as an anti-oncogene product, FEZ1 (fasciculation and elongation protein zeta-1) (Ishii et al., 2001). Here, we report the critical involvement of this protein in spine maturation. We also demonstrate the collaboration of PSD-Zip70 with its binding partner, SPAR, in spine maturation. This report also introduces the technique of *in utero* electroporation to investigate spine maturity *in vitro* and *in vivo*.

Received Sept. 22, 2004; revised Dec. 15, 2004; accepted Dec. 16, 2004.

This work was supported by Grant-in-Aid 15GS0312 for Scientific Research from the Ministry of Education, Science, Sports, and Culture of Japan (K.S.).

Correspondence should be addressed to Kenji Sobue, Department of Neuroscience (D13), Osaka University Graduate School of Medicine, 2-2, Yamadaoka, Suita City, Osaka 565-0871, Japan. E-mail: sobue@nbiochem.med.osaka-u.ac.jp.

DOI:10.1523/JNEUROSCI.3920-04.2005

 0270-6474/05/251421-10$15.00/0

Materials and Methods

Primary antibodies. The anti-bassoon mAb, which was isolated from a hybridoma cell line (336H), was cloned by the same procedure as described previously (Sun et al., 1998). The anti-SPAR polyclonal antibody (pAb) was produced by immunizing the MBP (myelin basic protein)-fused GK-binding domain of SPAR (SPAR-GKBD) in guinea pigs. The antiserum was exhaustively preabsorbed with MBP protein, followed by purification using a MBP-SPAR-GKBD-coupled Sepharose 4B gel matrix. Other primary antibodies used for immunocytochemistry were as follows: rabbit anti-PSD-Zip70 (Konno et al., 2002) and anti-GFP (Molecular Probes, Eugene, OR) pAbs; mouse anti-PSD-95 mAb (Affinity BioReagents, Golden, CO); anti-FLAG mAb (Sigma, St. Louis, MO), anti-Myc mAb (Santa Cruz Biotechnology, Santa Cruz, CA); and anti-GFP mAb (Molecular Probes).

Plasmid construction. To construct the expression vectors encoding PSD-Zip70 variants using pCAGGS, a mammalian expression vector driven by chicken β-actin promoter, the cDNAs were amplified by PCR and subcloned into pCAGGS using wild-type pcDNA3.1(+)-PSD-Zip70-Myc, as described previously (Konno et al., 2002), as a template. To isolate the full-length cDNA of SPAR, the adult rat brain cDNA library (Konno et al., 2002) was screened with the cDNA probe corresponding to SPAR-GKBD, and two positive clones containing the open reading frame (ORF) of full-length SPAR were isolated. The wild-type SPAR, SPAR-ΔGKBD (lacking GKBD; residues 1–1583), and GKBD (residues 1584–1783) were subcloned into FLAG-tagged pcDNA3.1(+) and pCAGGS expression vectors. The GFP expression vector was also constructed using pCAGGS. To generate the short-hairpin RNA constructs, the following DNA oligonucleotides were annealed and subcloned into the *Bsp*MI sites of the piGENEmU6 vector (Clontech, Cambridge, UK): 5′-GTTTGCTCAACCGGTACTCAGATGGTTCAAGAGACCATCTGAGTACCGGTTGAGCTTTTT-3′ and 5′- ATGCAAAAAGCTCAACCGGTACTCAGATGGTCTCTTGAACCATCTGAGTACCGGTTGAGC-3′ (corresponding to nucleotides 99–119 of the rat PSD-Zip70 ORF, as pmU6-Zip70–1); 5′- GTTTGGCTCTGTCATTCTCTGATGGTTCAAGAGACCATCAGAGAATGACAGAGCCTTTTT-3′ and 5′- ATGCAAAAAGGCTCTGTCATTCTCTGATGGTCTCTTGAACCATCAGAGAATGACAGAGCC-3′ (corresponding to nucleotides 684–704 of the rat PSD-Zip70 ORF, as pmU6-Zip70–2); and 5′- GTTTGGCACAGCTGAAGGACACCCGTTCAAGAGACGGGTGTCCTTCAGCTGTGCCTTTTT-3′ and 5′- ATGCAAAAAGGCACAGCTGAAGGACACCCGTCTCTTGAACGGGTGTCCTTCAGCTGTGCC-3′ (corresponding to nucleotides 1242–1262 of the rat PSD-Zip70 ORF, as pmU6-Zip70–3). The constructs were confirmed by DNA sequencing.

In utero *electroporation.* The details of the *in utero* electroporation have been described previously (Konno et al., 2005). In brief, pregnant ICR mice (Japan SLC, Shizuoka Ken, Japan) were anesthetized with sodium pentobarbital at 60 μg/g of body weight, and the uterine horns were exposed. Approximately 2–4 μg of indicated expression vectors were injected into the left lateral ventricle of the mouse embryonic brain [at embryonic day 13.5 (E13.5) for *in vivo* analyses or E15.5 for cell culture analyses] with a glass micropipette. The embryos in the uterus were placed between a tweezer-type electrode, which has 5-mm-diameter disc electrodes at the tip. Electronic pulses (30 V at E13.5 or 50 V at E15.5; 50 ms) were delivered five times at intervals of 950 ms with an electroporater (BTX830; BTX, Hawthorne, NY). The uterine horns were then placed back into the abdominal cavity to allow the embryos to continue normal development. The surgery as described above conformed to the guidelines for animal experiments of the Osaka University School of Medicine.

Cell culture. Mouse cerebral regions cotransfected with expression vectors by *in utero* electroporation were cultured at E16.5. Cultured neurons for microinjection were prepared from rat hippocampi at E18 (Konno et al., 2002; Usui et al., 2003). The mouse cerebral regions and the rat hippocampi were dispersed with 0.25% trypsin in HBSS. The dispersed neurons were plated on coverslips coated with 0.5 mg/ml poly-L-lysine (Sigma) at a density of 7500–10,000 cells/cm^2 and maintained in glial-conditioned MEM containing 2% B27 supplement (Invitrogen, San Diego, CA). One-half of the medium was changed to neurobasal medium (Invitrogen) containing 2% B27 supplement and 0.5 mM L-glutamine once per week (Konno et al., 2002; Usui et al., 2003).

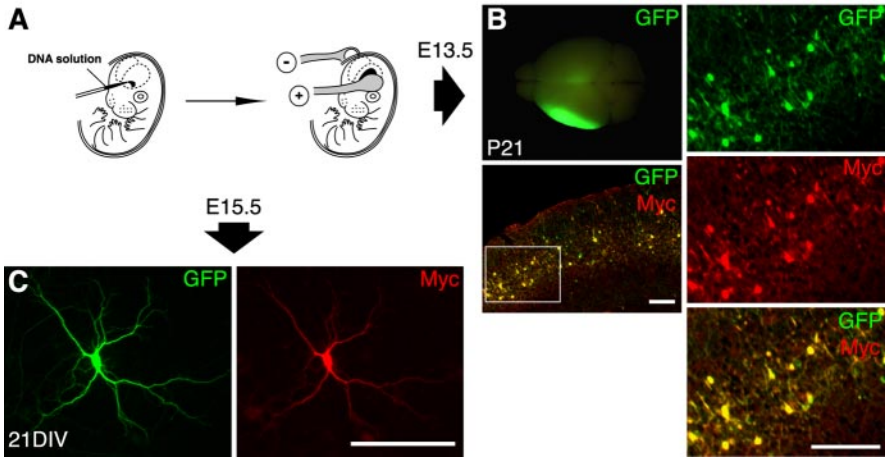

Figure 1. The *in utero* electroporation procedure and its application in this study. *A*, Scheme of the *in utero* electroporation procedure. Expression vectors were injected into the left lateral ventricle of embryonic brains (left) and transfected into neuronal progenitor cells by *in utero* electroporation (right). *B*, GFP fluorescence in a rat brain (at P21) cotransfected with expression vectors encoding GFP and Myc-tagged PSD-Zip70C (left, top). A merged image of the thin section of the forebrain at P21 was double immunostained for GFP and Myc (left, bottom). High-magnification views of the segment enclosed in a white box are shown in the right column. *C*, Immunolabeling for GFP (left) and Myc (right) in cultured neurons (21 DIV) from the cerebral regions electroporated with GFP and Myc-tagged PSD-Zip70C expression vectors. Scale bars, 200 μm.

Microinjection. Using a micromanipulator (Narishige, Tokyo, Japan), indicated expression vectors (10–50 ng/μl) were microinjected through a glass capillary into the nuclei of rat hippocampal neurons at 21–28 days *in vitro* (DIV) (Konno et al., 2002; Usui et al., 2003). After 24 or 72 h, the neurons were fixed for immunocytochemistry as described below.

Immunocytochemistry. For all immunostaining except F-actin, the neurons were fixed with 4% paraformaldehyde in PBS containing 4% sucrose for 1 h at 4°C. After fixation, the neurons were treated at 4°C for 20 min with methanol precooled at −20°C. For F-actin labeling, the neurons were fixed with 4% paraformaldehyde in PBS containing 4% sucrose for 15 min at room temperature. Immunostaining was performed as described previously (Konno et al., 2002). In brief, the neurons were permeabilized with 0.25% Triton X-100 for 10 min, incubated in the blocking solution (5% normal goat serum, 1% bovine serum albumin, and 0.05% Triton X-100 in PBS) for 1 h at 37°C, and immunolabeled with primary antibodies in the same blocking solution overnight. Then the neurons were labeled with Alexa Fluor 488- and 546-conjugated secondary antibodies (2 μg/ml; Molecular Probes) in the blocking solution for 1 h at room temperature. For F-actin staining, the neurons were incubated with Alexa Fluor 568-conjugated phalloidin (2 μg/ml; Molecular Probes) in 3% BSA for 30 min at room temperature.

Immunohistochemistry. After the *in utero* electroporation of indicated expression vectors at E13.5, mice at postnatal day 21 (P21) were deeply anesthetized with pentobarbital and perfused transcardially with ice-cold 0.9% saline, followed by 4% paraformaldehyde in PBS. After the brains were dissected, they were further fixed in the same buffer for 4 h at 4°C, immersed in 25% sucrose in PBS overnight at 4°C, and then embedded in OCT compound (Miles, Elkhart, IN). Coronal sections (5–20 μm thick) were prepared using a cryostat. Before immunostaining, the sections were rehydrated in PBS at room temperature. The sections were permeabilized with the blocking solution containing 10% normal goat serum, 0.2% BSA, and 0.1% Triton X-100 in 0.1 M PBS for 1 h at 37°C, and

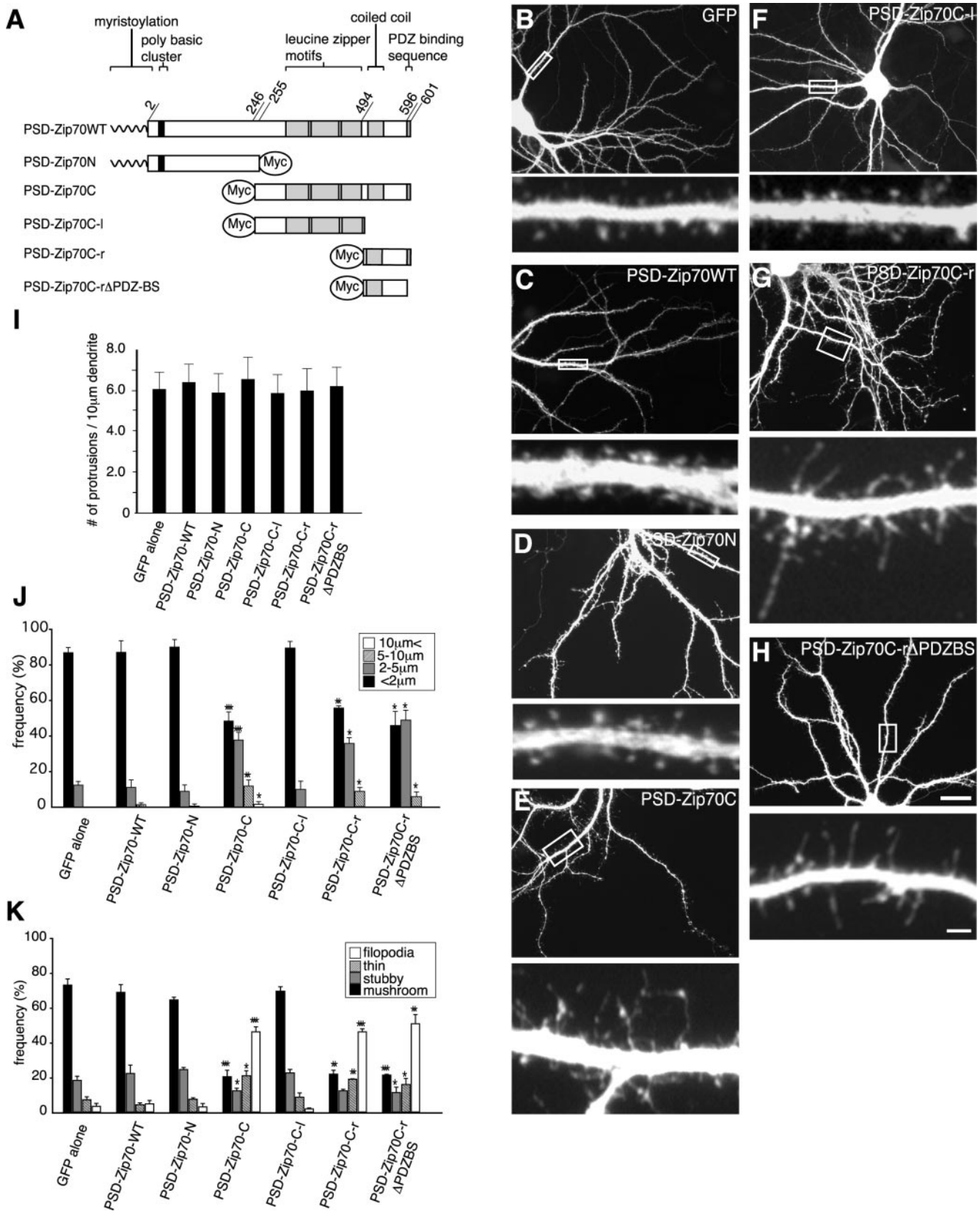

Figure 2. Effects of PSD-Zip70 variants on spine morphology *in vitro*. *A*, The PSD-Zip70 variants used in this study. *B–H*, GFP fluorescence images of the dendrites from cortical neurons in culture. GFP alone or GFP and Myc-tagged PSD-Zip70 variants were introduced into neuronal progenitor cells by *in utero* electroporation. In the following figures, high-magnification views of the dendritic segments enclosed in white boxes are shown at bottom of each panel. *I–K*, Quantitative analyses of the protrusion density (*I*), length (*J*), and morphology (*K*) of neurons expressing GFP alone or GFP and PSD-Zip70 variants. One thousand dendritic protrusions of 10 neurons expressing GFP alone, PSD-Zip70WT, PSD-Zip70N, and PSD-Zip70C were quantified, and 800 dendritic protrusions of 8 neurons expressing PSD-Zip70CI, PSD-Zip70Cr, and PSD-Zip70Cr-ΔPDZBS were quantified ($n = 10$ experiments). Mean ± SD; *$p < 0.05$, **$p < 0.001$, and ***$p < 0.0001$ compared with GFP alone (Student's *t* test). Scale bars: *H*, bottom, 2 μm; *H*, top, 20 μm.

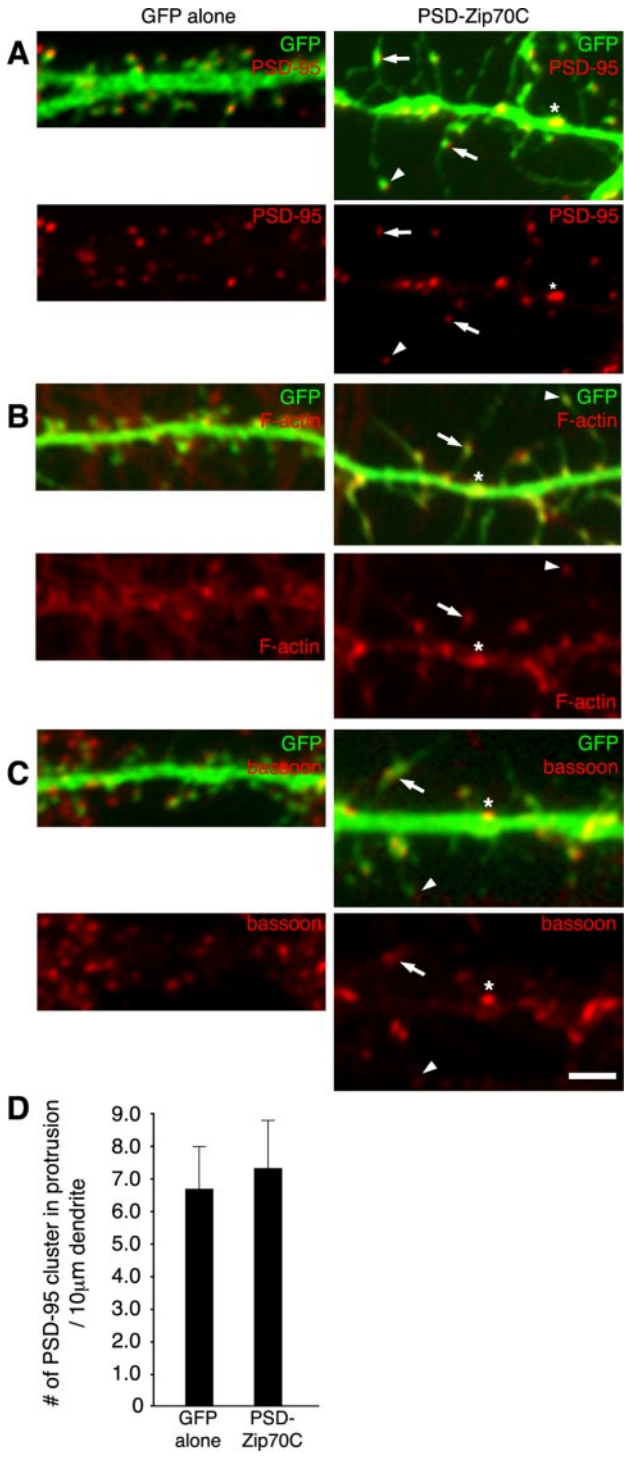

Figure 3. Characterization of PSD-Zip70C-induced elongated spines. Neurons transfected with GFP alone (left) or GFP and PSD-Zip70C (right) at 21 DIV were immunostained for GFP and PSD-95 (*A*), F-actin (*B*), or bassoon (*C*). The small head of thin spines (arrowhead), midbody of long filopodia (arrow), and shaft spine (asterisk) are indicated. *D*, Quantitative analysis of the number of PSD-95 clusters in protrusions per 10 μm dendrite from neurons transfected with GFP alone or GFP and PSD-Zip70C (each sample was quantified along a 100 μm dendrite of one neuron, and the number of PSD-95 clusters in protrusions was expressed as PSD cluster per 10 μm dendrite; $n = 5$ neurons) (mean ± SD). Scale bar, 2 μm.

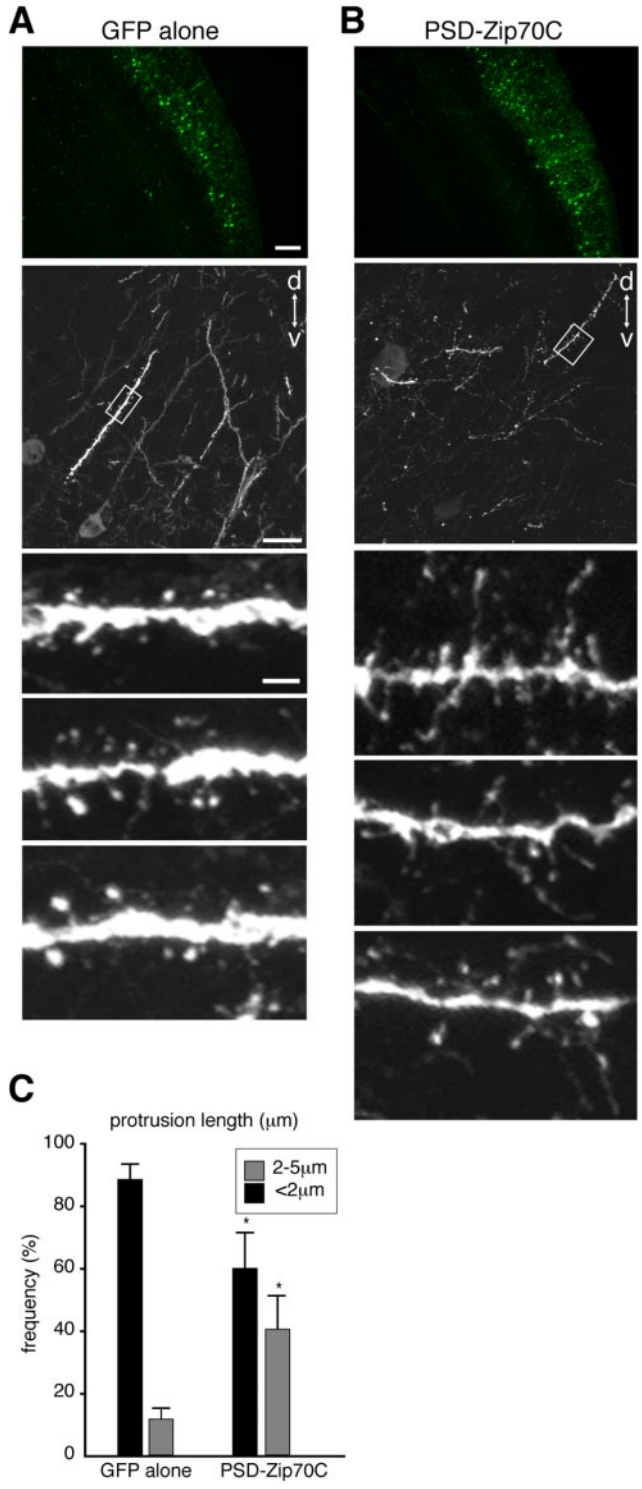

Figure 4. Inhibition of mature spine formation by PSD-Zip70C *in vivo*. *A*, *B*, GFP fluorescence images of neurons expressing GFP alone (*A*) or GFP and PSD-Zip70C (*B*). *C*, Quantitative analysis of the length of dendritic protrusions from neurons expressing GFP alone or GFP and PSD-Zip70C (each sample was quantified with 500 spines; $n = 4$ experiments). Mean ± SD; *$p < 0.05$ compared with GFP alone (Student's *t* test). Scale bars: *A*, bottom, 2 μm; *A*, middle, 20 μm; *A*, top, 200 μm. d, Dorsal, v, ventral.

immunolabeled with primary antibodies in the same blocking solution overnight. The anti-GFP pAb and anti-Myc mAb were used as primary antibodies. After washing with 0.1 M PBS for 30 min, the sections were incubated with Alexa Fluor 488 and 546 secondary antibodies for 2 h at room temperature.

Microscopy and quantification analyses. Immunofluorescence images were acquired with a cooled CCD camera (Roper Scientific, Trenton, NJ) mounted on an Olympus Optical (Tokyo, Japan) IX70 microscope. To obtain projections of confocal images, the images were acquired with an

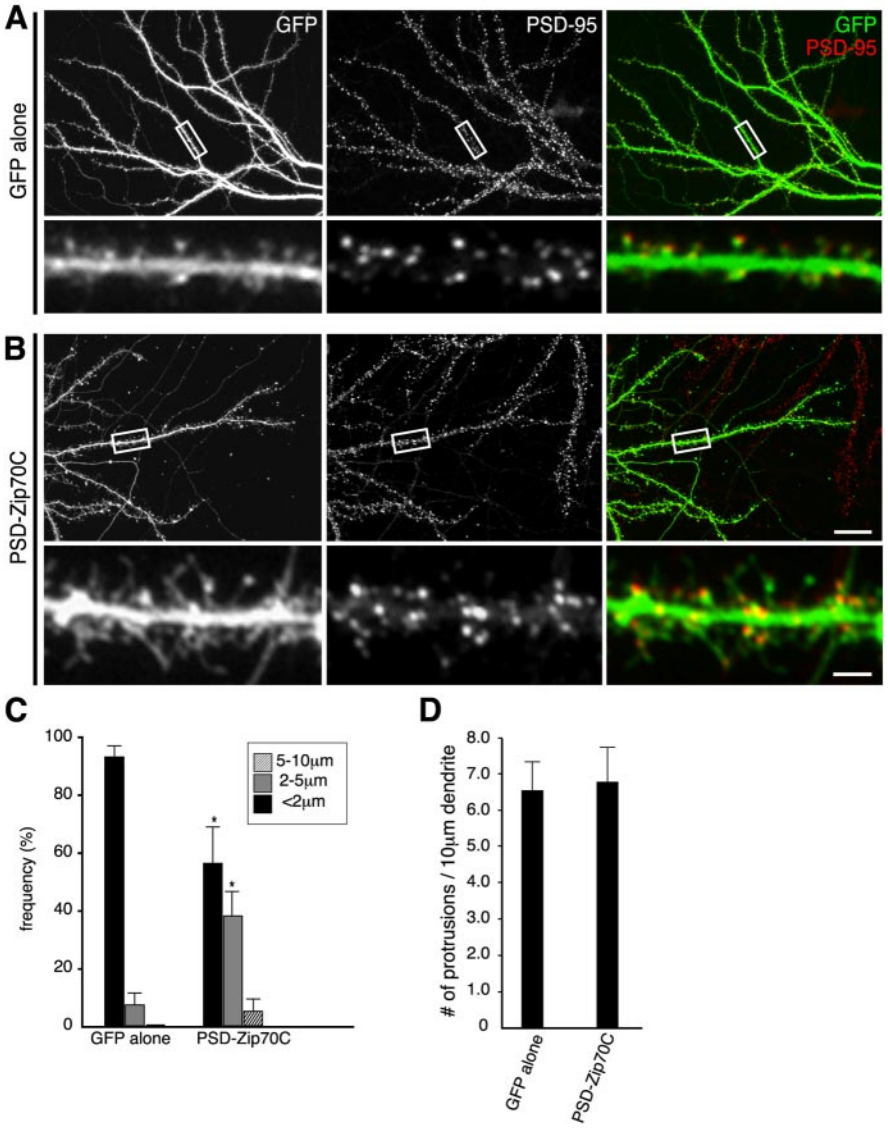

Figure 5. Effect of transiently overexpressed PSD-Zip70C on spine morphology. GFP alone (*A*) or GFP and PSD-Zip70C (*B*) were overexpressed in mature hippocampal neurons (21 DIV) by microinjection of their expression vectors. Neurons were immunostained for GFP and PSD-95. *C*, *D*, Quantitative analyses of the length (*C*) and density (*D*) of dendritic protrusions from neurons expressing GFP alone or GFP and PSD-Zip70C (each sample was quantified with 800 protrusions from 8 neurons; $n = 10$ experiments). Mean ± SD; $*p < 0.05$ compared with GFP alone (Student's *t* test). Scale bars: *B*, bottom, 2 μm; *B*, top, 20 μm.

LSM5Pascal confocal microscope system (Zeiss, Oberkochen, Germany), and stacked images were constructed from the optical slices at 0.36 μm and then projected into one image. For the quantification of spine density, the number of protrusions in the dendrites between the first branch point and the second branch point were counted. The maximum length and width of each protrusion were manually measured with the aid of MetaMorph Software (Universal Imaging Corporation, West Chester, PA). Morphological categories of spine shape were defined as follows. Mushroom spines (<2 μm in length and >0.5 μm in width) have spine neck. Stubby spines (<2 μm in length and >0.5 μm in width) do not have spine neck. Thin spines (<2 μm in length and <0.5 μm in width) show the small head with thin spine neck. Filopodia (>2 μm in length and <0.5 μm in width) do not have the spine head. Neurons for morphometric analyses were randomly sampled from each neuronal preparation.

Immunoprecipitation. The brain extracts in radioimmunoprecipitation assay (RIPA) buffer [50 mM Tris-HCl, 150 mM NaCl, 5 mM EDTA, 1% Triton X-100, 0.5% deoxycholate, 0.1% SDS, and protease inhibitors (Roche Products, Welwyn Garden City, UK), pH 7.2] were preabsorbed with protein A-Sepharose, reacted with anti-PSD-Zip70 or anti-SPAR antibodies or normal rabbit IgG, and further reacted with protein A-Sepharose. The proteins immunoprecipitated were analyzed by immunoblotting using anti-PSD-Zip70 and anti-SPAR antibodies. The COS-7 cell extracts coexpressing PSD-Zip70-Myc and FLAG-tagged full-length SPAR (FLAG-SPAR-WT) or FLAG-SPAR-ΔGKBD in RIPA buffer were immunoprecipitated with anti-Myc or anti-FLAG antibodies using the procedure described above.

Ligand overlay binding assay. Glutathione *S*-transferase (GST)-fused full-length PSD-Zip70 (PSD-Zip70WT), the N terminus of PSD-Zip70 (PSD-Zip70N), the C terminus of PSD-Zip70 (PSD-Zip70C), the left-side region of the C terminus of PSD-Zip70 (PSD-Zip70C-l), and the right-side region of the C terminus of PSD-Zip70 (PSD-Zip70C-r), and MBP-fused SPAR-GKBD, the N-terminal half of SPAR-GKBD (SPAR-GKBD-N), and the C-terminal half of SPAR-GKBD (SPAR-GKBD-C) were expressed in *Escherichia coli* BL21 and isolated using glutathione-conjugated Sepharose 4B (Amersham Biosciences, Arlington Heights, IL) and amylose resin (New England Biolabs, Beverly, MA). Equal amounts of the brain subcellular fractions and MBP-fused proteins were loaded on gels, separated by SDS-PAGE, and transferred to nitrocellulose membranes. The membranes were blocked with 5% skim milk in TBS and Tween 20 (TBST) and then incubated with or without purified GST-fusion proteins (0.5 μg/ml) in the same buffer for 2 h at room temperature. After washing with TBST, the proteins were visualized by immunoblotting using anti-GST or anti-MBP pAbs as primary antibodies.

Isolation and identification of a PSD-Zip70 binding partner. The PSD fraction prepared from adult rat brains was extracted with 2% *N*-lauroyl sacrosinate solution. The extract was diluted with 10 vol of binding buffer (in mM: 20 Tris-HCl, 1 EDTA, 100 NaCl, and 2 β-mercaptoethanol, pH 7.4), dialyzed with the same buffer, and then applied to a GST-fused PSD-Zip70C affinity column. After washing with the binding buffer, proteins eluted with SDS sample buffer were separated by SDS-PAGE. The gel containing a 200 kDa protein was cut out and digested with lysyl endopeptidase. The digested peptides were separated by liquid column chromatography. The amino acid sequences of two peptides were determined with a peptide Sequencer.

Results

In utero electroporation of expression vectors

To investigate the importance of PSD-Zip70 in spine dynamics *in vitro* and *in vivo*, we developed the technique of *in utero* electroporation, in which expression vectors encoding GFP and PSD-Zip70 variants were cotransfected into neuronal progenitor cells lining the ventricular zone of mouse brains at E13.5 (Fig. 1). Using this technique, we could control the expression level, rate, and cerebral location of the exogenous proteins *in vivo*. By exposing the surface of the cerebral cortex to excitation luminescence, we could easily detect GFP-positive neuron-enriched cerebral regions at P21. In thin section of this region, GFP- and Myc-tagged PSD-Zip70 variant-positive neurons were precisely local-

ized to layers II/III of the cerebral cortex. In this experiment, we used PSD-Zip70C. In the *in vitro* experiments, *in utero* electroporation was performed at E15.5. Neurons in the cerebral regions that were cotransfected were cultured the next day (E16.5). By 21 DIV, GFP and PSD-Zip70C were still highly coexpressed in the cerebral neurons (96.2 ± 2.2% of the GFP-positive cells coexpressed Myc-tagged PSD-Zip70C; mean ± SD; 300 neurons; $n = 3$ experiments). In the following experiments, we used GFP to identify neurons expressing PSD-Zip70 variants and to monitor the outline of spines and dendrites. As shown in Figures 1–4 (see also Fig. 9), the PSD-Zip70 variants did not affect the dendritic outgrowth or branching of cerebral neurons *in vitro* or the neuronal migration from the ventricular zone to layers II/III of the cerebral cortex *in vivo*.

Inhibition of mature spine formation induced by PSD-Zip70 variants *in vitro* and *in vivo*

Using this technique, we first analyzed the effects of PSD-Zip70 variants on spine morphology *in vitro*. By 21 DIV, most of the spines from neurons overexpressing full-length PSD-Zip70 (PSD-Zip70WT) and its N terminus (PSD-Zip70N) showed a mushroom-shaped short form (Fig. 2*C*,*D*). There were no significant differences in spine morphology (shape, size, or length) among neurons expressing GFP with or without PSD-Zip70WT or PSD-Zip70N (Fig. 2*B–D*). Furthermore, neither exogenous PSD-Zip70WT nor PSD-Zip70N affected the localization of the postsynaptic markers PSD-95 and F-actin in spines (data not shown). These results indicated that neither PSD-Zip70WT nor PSD-Zip70N had any effect on spine morphology. In contrast, the PSD-Zip70C-positive neurons showed a marked increase in thin spines and long filopodia concomitant with a decrease in mushroom-shaped short spines (Fig. 2*E*). Within the C terminus, the right-side region (PSD-Zip70C-r) and the same region with the PDZ-binding sequence deleted (PSD-Zip70C-rΔPDZBS), but not its left-side region (PSD-Zip70C-l), also markedly induced thin spine and long filopodia formation with a decrease in mushroom-shaped short spines (Fig. 2*F–H*). In all of these experiments, the PSD-Zip70 variants had no significant effect on the total number of spines (Fig. 2*I*). The length of spines from the base of the neck to the spine head was measured, and the spine shape was classified for each experiment (Fig. 2*J*,*K*). These results indicate that PSD-Zip70C, especially its short C-terminal region (residues 495–596) containing the coiled-coil domain, displays a dominant-negative function of the parent molecule, resulting in the inhibition of mature spine formation. In the following experiments, we used PSD-Zip70C as a representative dominant-negative mutant.

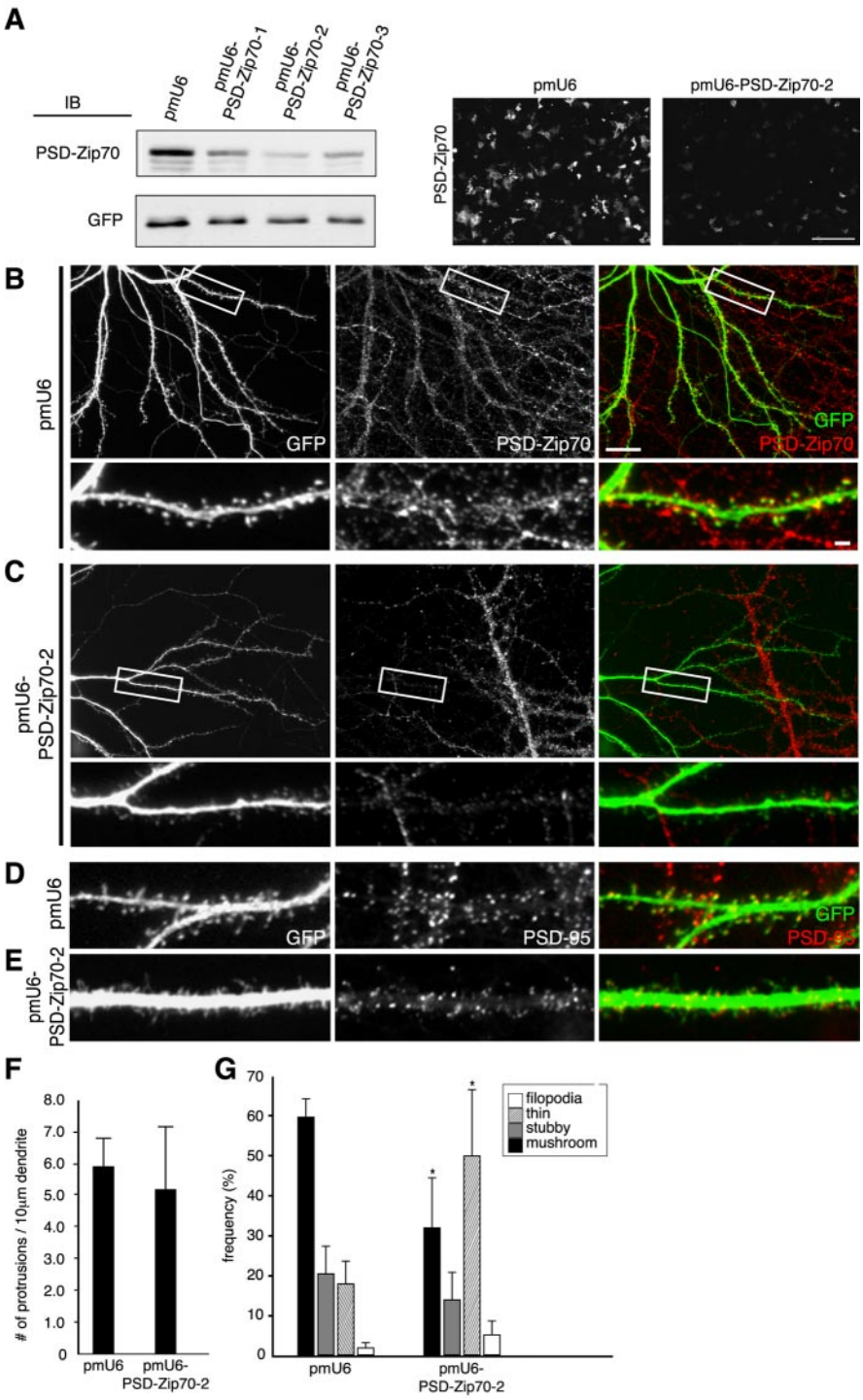

Figure 6. Effect of PSD-Zip70 knock-down on spine morphology. *A*, COS-7 cells cotransfected with GFP and Zip70WT expression vectors and pmU6 or pmU6-Zip70 –1 to pmU6-Zip70 –3 vectors were analyzed by immunoblotting (IB, left) and immunostaining (right) for GFP and/or PSD-Zip70. Scale bar, 200 μm. *B–E*, Hippocampal neurons (21 DIV) cotransfected with GFP and pmU6 or pmU6-Zip70 –2 were double stained for GFP and PSD-Zip70 or PSD-95. *F*, *G*, Quantification of the spine density (number of spines per 10 μm dendrite length) (*F*) and morphology (*G*) (each sample was quantified with 1000 protrusions from 10 neurons; $n = 10$ experiments). Mean ± SD; $^*p < 0.05$ compared with GFP alone (Student's *t* test). Scale bars: *B*, bottom, 2 μm; *B*, top, 20 μm.

To characterize the PSD-Zip70C-induced thin spines and

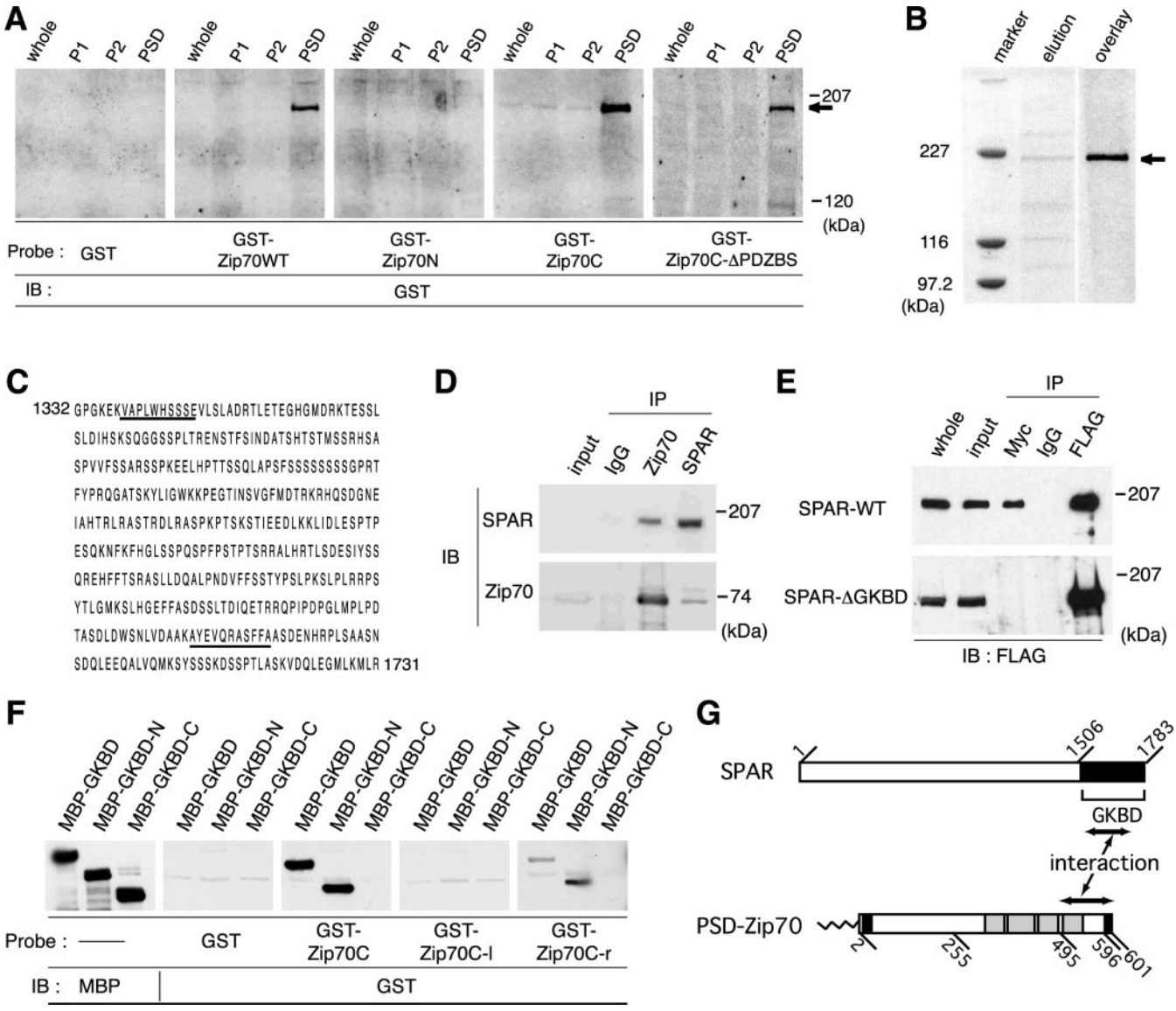

Figure 7. Identification of SPAR as the PSD-Zip70 binding partner. *A*, Ligand overlay binding assay to identify PSD-Zip70 binding partner(s). The indicated GST-fusion proteins were used as ligands. Bound GST-fusion proteins were visualized by immunoblotting (IB). The arrow indicates a 200 kDa PSD protein. Whole, P1, S2, and PSD indicate the whole-brain lysate, crude membrane, soluble, and PSD fractions, respectively. *B*, Partial purification of a 200 kDa PSD protein using a GST-fused PSD-Zip70C affinity column. A partially purified 200 kDa PSD protein (arrow) was stained with Coomassie brilliant blue (elution) and detected by ligand overlay assay using GST-fused PSD-Zip70C as a ligand (overlay). *C*, Amino acid sequences of the SPAR C-terminal region. Underlining indicates partial sequences of two peptides from the 200 kDa PSD protein. *D*, Coimmunoprecipitation of PSD-Zip70 and SPAR from the brain extracts. The brain extracts were coimmunoprecipitated (IP) with anti-PSD-Zip70 or anti-SPAR antibodies or normal rabbit IgG and were analyzed by immunoblotting (IB) for SPAR or PSD-Zip70. *E*, *In vitro* interaction between PSD-Zip70 and SPAR. The COS-7 cell lysates cotransfected with PSD-Zip70-Myc and FLAG-SPAR-WT or FLAG-SPAR-ΔGKBD were immunoprecipitated (IP) with anti-Myc or anti-FLAG antibodies and analyzed by immunoblotting (IB) for FLAG. *F*, Ligand overlay binding assay to determine the binding domains of PSD-Zip70 and SPAR. GKBD, GKBD-N, and GKBD-C indicate the regions corresponding to residues 1583–1783, 1584–1714, and 1715–1783 of SPAR, respectively. Zip70C, Zip70C-I, and Zip70C-r indicate the regions corresponding to residues 246–601, 246–494, and 495–601 of PSD-Zip70, respectively. GST, GST-Zip70C, GST-Zip70C-I, and GST-Zip70C-r were used as ligands. GKBD-C and GKBD-N indicate the C-terminal and N-terminal halves of SPAR-GKBD. *G*, Schematic diagram of the interaction between PSD-Zip70 and SPAR.

long filopodia, we analyzed the localization of postsynaptic and presynaptic proteins (Fig. 3). Immunoclusters for PSD-95, F-actin, and bassoon were localized to the small head of the thin spines and the midbody of the long filopodia. Some clusters of postsynaptic or presynaptic proteins along the dendrites were also observed. However, there were no significant differences in the number of PSD-95 clusters in dendritic protrusions from the neurons transfected with GFP alone or PSD-Zip70C (Fig. 3*D*). Together, these results indicate that PSD-Zip70C and its deletion mutants only affect spine morphology, but not spine number, *in vitro*.

We further analyzed the effect of PSD-Zip70C on spine morphology *in vivo*. After *in utero* electroporation at E13.5, migrating neurons coexpressing GFP and PSD-Zip70C were detected within the intermediate zone at E15.5. These neurons reached the cortical plate and were finally localized to layers II/III of the cerebral cortex before P2 (data not shown). It is well known that synaptogenesis in the mouse cerebral cortex dramatically increases at P11–P30 (Lendval et al., 2000; Grutzendler et al., 2002). We therefore analyzed the spine morphology of GFP-positive neurons in layers II/III of the cerebral cortex at P21 (Fig. 4). Neurons expressing GFP alone had mainly mushroom-shaped

short spines. Consistent with the *in vitro* experiments (Figs. 2, 3), GFP- and PSD-Zip70C-positive neurons showed a marked increase in thin spines and long filopodia and a decrease in mushroom-shaped short spines. These results indicate that PSD-Zip70C also inhibit mature spine formation *in vivo*.

Destabilization of mature spines induced by PSD-Zip70 mutant

Using a microinjection technique, we then introduced expression vectors encoding GFP with or without PSD-Zip70C into mature neurons in culture (21 DIV) and analyzed the spine morphology (Fig. 5). Consistent with the *in utero* electroporation experiments, PSD-Zip70C markedly induced thin spines and long filopodia in association with a decrease in mushroom-shaped short spines within 24 h after the microinjection. In this experiment, PSD-Zip70C had no effect on the total number of spines (Fig. 5*D*) and dendritic outgrowth and branching. These results indicate the destabilization of preformed mature spines by PSD-Zip70C.

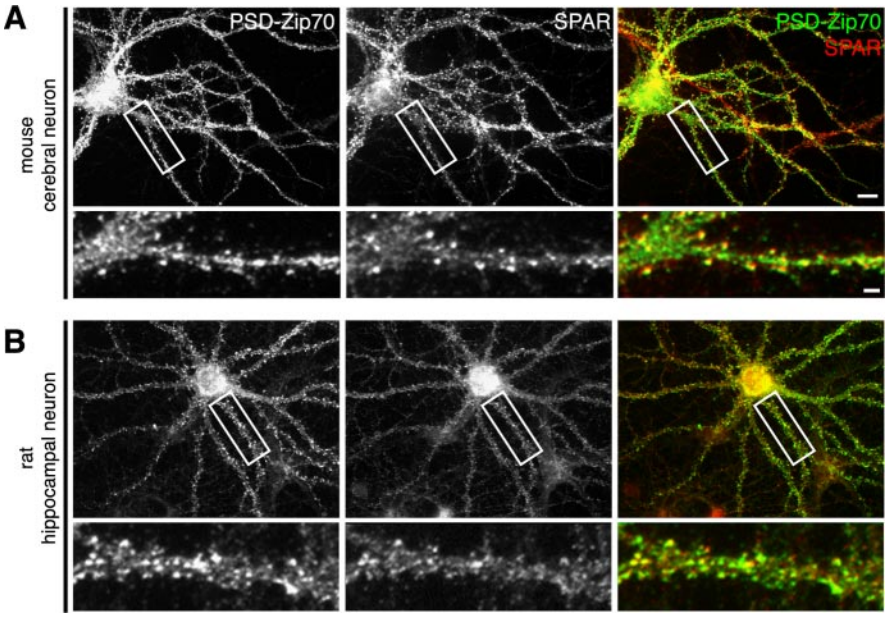

Figure 8. Localization of PSD-Zip70 and SPAR in cultured neurons. The localization of endogenous PSD-Zip70 and SPAR in mouse cerebral (*A*) and rat hippocampal (*B*) neurons in culture. Scale bars: *A*, bottom, 2 μm; *A*, top, 20 μm.

Effect of PSD-Zip70 knock-down on spine morphology

Because the above experiments showed the dominant-negative effects of PSD-Zip70C and its deletion mutants on spine morphology, we next used the strategy of interfering with the expression of PSD-Zip70 in mature neurons in culture. Three vectors encoding short-hairpin RNAs (pmU6-Zip70–1, pmU6-Zip70–2, and pmU6-Zip70–3) were designed from the cDNA-coding region of rat PSD-Zip70. Of these, pmU6-Zip70–2 most successfully reduced the level of exogenous PSD-Zip70 protein in COS-7 cells, as determined by immunoblotting and immunocytochemistry (Fig. 6*A*). pmU6-Zip70–2 or the empty vector (pmU6) was introduced along with the GFP expression vector into mature neurons by microinjection. pmU6-Zip70–2, but not pmU6, strongly suppressed the expression of the endogenous PSD-Zip70 protein and markedly increased the thin spines in association with a decrease in the mushroom-shaped ones (Fig. 6*B*–*G*). There were, however, no significant differences in the number of PSD-95 clusters in dendritic protrusions from neurons transfected with pmU6 or pmU6-PSD-Zip70–2 [the number of PSD-95 clusters in protrusions per 10 μm dendrite; pmU6, 6.23 $\pm$ 0.58 and pmU6-PSD-Zip70–2, 7.10 $\pm$ 1.57 (mean $\pm$ SD); $p > 0.05$ (Student's *t* test); $n = 5$ neurons]. These results indicate that the knock-down of PSD-Zip70 causes the destabilization of mature spines.

PSD scaffold protein, SPAR, as a binding partner of PSD-Zip70

To search for the binding partners of PSD-Zip70 in the formation of mature spines, we performed ligand overlay binding assays using GST-fused PSD-Zip70 variants (Fig. 7*A*). GST-fused PSD-Zip70WT and PSD-Zip70C, but not PSD-Zip70N and PSD-Zip70C-rΔPDZBS, bound specifically to a protein with a molecular mass of 200 kDa that was highly concentrated in the PSD fraction. In this assay, the 200 kDa PSD protein was the only PSD-Zip70 binding partner found in the PSD fraction. We partially purified this protein from PSD extracts using a GST-fused PSD-Zip70C affinity column (Fig. 7*B*) and sequenced two of its proteolytic fragments. Two partial sequences of these fragments corresponded to residues 1338–1347 and 1667–1676 of the PSD scaffold protein SPAR (Fig. 7*C*).

To verify the interaction between PSD-Zip70 and SPAR and to identify their interacting domains, we performed coimmunoprecipitation and ligand overlay binding assays. Anti-PSD-Zip70 and anti-SPAR antibodies coimmunoprecipitated SPAR and PSD-Zip70, respectively, from brain extracts (Fig. 7*D*), suggesting a physical interaction. The PSD-Zip70 and SPAR interaction was confirmed by a coimmunoprecipitation assay using COS-7 cell extracts cotransfected with Myc-tagged Zip70WT and FLAG-tagged full-length SPAR (SPAR-WT); no such interaction was found for GK-binding domain-deleted SPAR (SPAR-ΔGKBP) (Fig. 7*E*). Ligand overlay binding assays revealed that GST-fused PSD-Zip70C and PSD-Zip70C-r, but not PSD-Zip70C-l, bound to the MBP-fused GK-binding domain of SPAR (MBP-GKBD) and its N-terminal half (MBP-GKBD-N), but not its C-terminal half (MBP-GKBD-C) (Fig. 7*F*). These results indicate that the PSD-Zip70 and SPAR interaction is mediated through the short C-terminal region of PSD-Zip70 containing the coiled-coil domain and the N-terminal half of the SPAR GK-binding domain (Fig. 7*G*).

PSD-Zip70 and SPAR interaction in spine morphology

We further investigated the significance of the PSD-Zip70 and SPAR interaction in the spine morphology. We compared the localization of PSD-Zip70 and SPAR in mouse cortical and rat hippocampal neurons in culture (Fig. 8). In both neurons, the SPAR immunoclusters in the spines were colocalized with PSD-Zip70 clusters.

We then investigated the significance of PSD-Zip70-SPAR interaction in spine morphology. First, we examined the effect of PSD-Zip70C on the localization of SPAR by *in utero* electroporation (Fig. 9*A*,*B*). Consistent with the PSD-Zip70C-induced thin spines and long filopodia associated with a decrease in mushroom-shaped short spines (Figs. 2–4), SPAR lost its localization to the spine and instead was distributed diffusely within

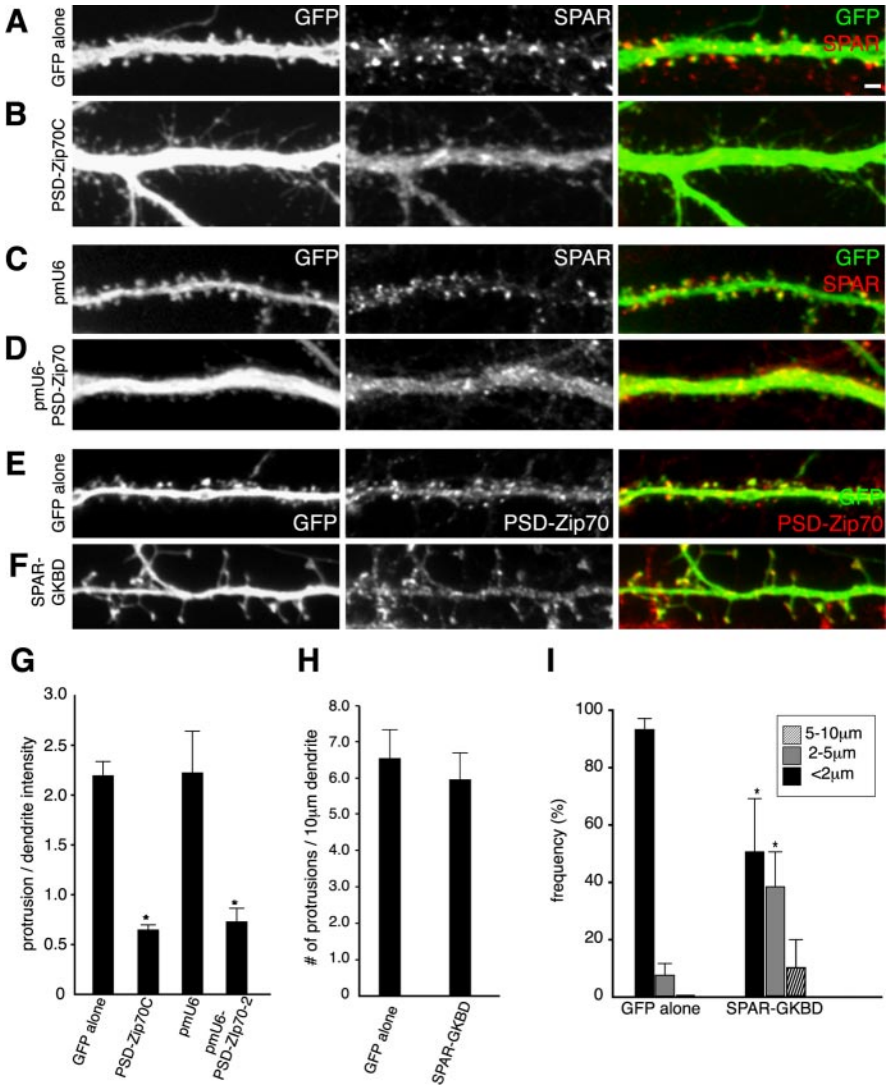

Figure 9. Significance of PSD-Zip70 and SPAR interaction in spine morphology. The GFP expression vector alone (*A*) or GFP and PSD-Zip70C (*B*) were overexpressed in cortical neurons (21 DIV) by *in utero* electroporation. Neurons were immunostained for GFP or SPAR. The GFP expression vector and pmU6 (*C*) or pmU6-PSD-Zip70 –2 (*D*) were cotransfected into hippocampal neurons (21 DIV) by microinjection. Neurons were immunostained for GFP or SPAR. GFP alone (*E*) or GFP and SPAR-GKBD (*F*) were overexpressed in hippocampal neurons (21 DIV) by microinjection. Neurons were immunostained for GFP or PSD-Zip70. *G*, The localization of SPAR in dendritic protrusions expressed as ratios of the fluorescence intensity of protrusion to that of shaft from neurons transfected with GFP alone, GFP and PSD-Zip70C, GFP and pmU6, or GFP and pmU6-PSD-Zip70 –2 (each sample was quantified with 500 protrusions from 5 neurons). *H*, *I*, Quantitative analyses of the density (*H*) or length (*I*) of protrusions from neurons expressing GFP alone or GFP and SPAR-GKBD (each sample was quantified with 800 protrusions from 8 neurons; $n = 10$ experiments). Mean ± SD; $^*p < 0.05$ compared with GFP alone (Student's *t* test). Scale bar (in *A*), 2 μm.

the dendrites. Second, the knock-down of PSD-Zip70 by pmU6-Zip70–2 also induced thin spines and the diffuse distribution of SPAR within the dendrites (Fig. 9*C*,*D*). Third, the overexpression of SPAR-GKBD by microinjection of its expression vector into mature neurons caused an increase in thin, long-necked spines (Fig. 9*E*,*F*,*H*,*I*). This result was consistent with that reported by Pak et al. (2001). Furthermore, PSD-Zip70 immunoclusters remained at the small heads of the thin, long-necked spines. Together, these results suggest that the interaction between PSD-Zip70 and SPAR is critically involved in the mature spine formation and the maintenance of spine maturity.

Discussion

It has been reported that the overexpression of PSD proteins, such as PSD-95 (El-Husseini et al., 2000), Kalirin (Penzes et al., 2001), Homer and Shank (Carlo et al., 2001), α- and β-catenins (Murase et al., 2002; Abe et al., 2004), and SPAR (Pak et al., 2001) enlarges the heads of mature spines, whereas their dominant-negative mutants transform mushroom-shaped spines to filopodia. Because most of these studies used mature neurons in culture, the results, however, represent the enlargement of mature spine heads by the overexpression of PSD proteins and the destabilization of mature spines by their dominant-negative mutants. PSD-Zip70 is predominantly expressed in the neurons of some cerebral regions. In spines, it is localized to the PSD and dendritic rafts. The N-terminal myristoylation and polybasic cluster of PSD-Zip70 are sufficient for its membrane localization, and its C terminus is required for spine targeting (Konno et al., 2002). In this study, we developed the technique of *in utero* electroporation and used it to investigate spine dynamics *in vitro* and *in vivo*. With this technique, exogenous proteins, such as GFP and PSD-Zip70 variants, were already expressed in premature migrating neurons, and their expression continued in neuronal cell culture and in layers II/III of the cerebral cortex *in vivo*. By changing the direction of electrode during *in utero* electroporation, the transfected proteins were expressed in neurons of intended cerebral regions. This technique can, therefore, enable us to observe the effects of PSD-Zip70 variants during synaptogenic processes. Using this technique, we demonstrated the inhibition of mature spine formation induced by the C-terminal variants of PSD-Zip70 *in vitro* and *in vivo*. Especially the short C-terminal region of PSD-Zip70C containing the coiled-coil domain was critically involved in the immature phenotype. We also showed the same phenotype by transient overexpression of PSD-Zip70C and knock-down of PSD-Zip70 in mature neurons. Together, these results suggest that PSD-Zip70 is critically involved in spine maturation. Thus, this is a first report introducing the technique of *in utero* electroporation to investigate spine maturity *in vitro* and *in vivo*.

SPAR was isolated as a multidomain PSD protein that interacts with PSD-95, the small GTPase Rap, and actin filaments and controls the shape change of spines by regulating actin filaments (Pak et al., 2001). Pak and Sheng (2003) recently showed that SPAR interacts with Snk (serum-inducible kinase) and that overexpression of Snk in heterologous cells leads to the degradation of SPAR. Furthermore, the neuronal activity-dependent expression of endogenous Snk eliminates SPAR, depletes PSD-95 and bassoon immunoclusters, and causes a loss of mature spines. From these findings, it has been hypothesized that a molecular mechanism underlying the structural plasticity of synapses in which Snk is targeted to spines and executes the degradation of PSD scaffold

proteins involved in spine dynamics (Meyer and Brose, 2003). As demonstrated here, PSD-Zip70 binds SPAR via a short C-terminal region of PSD-Zip70 and the C-terminal half of SPAR-GKBD. Furthermore, PSD-Zip70C and its short C-terminal region, which act as dominant-negative mutants of the PSD-Zip70 and SPAR interaction, inhibited the formation of mature spines *in vitro* and *in vivo*. The immature spine phenotype was also seen with the knock-down of PSD-Zip70. In both cases, SPAR lost its spine localization in association with the immature spine phenotype. Consistent with the data reported by Pak et al. (2001), the overexpression of SPAR-GKBD, which is also a dominant-negative mutant of the PSD-Zip70 and SPAR interaction, induced long-necked spines without affecting the localization of PSD-Zip70 in the small head of thin, long-necked spines. Together, our results indicate that the PSD-Zip70 and SPAR interaction mediated by the short C-terminal region of PSD-Zip70 and the C-terminal half of SPAR-GKBD in spines is critical for mature spine formation and suggest that the localization of PSD-Zip70 in the spine, in which it acts as an anchoring protein for SPAR, is a prerequisite for the PSD-Zip70/SPAR-linked spine maturation. Pak et al. (2001) also showed the enlargement of spine heads by the overexpression of SPAR. In our present study, the overexpression of PSD-Zip70WT had no significant effect on spine morphology, including enlargement of the spine heads. This inconsistency may be attributable to the presence of an excessively high level of PSD-Zip70 compared with the level of SPAR.

The dominant-negative strategy to prevent the PSD-Zip70 and SPAR interaction and the knock-down strategy for PSD-Zip70 showed, however, significantly different phenotypes of spine morphology. Although the former strategy is targeted to the interacting sites of the two proteins, overexpression of PSD-Zip70C and its deletion mutants markedly induced thin spines and long filopodia, and neurons overexpressing SPAR-GKBD showed the formation of thin, long-necked spines. Using the PSD-Zip70 knock-down strategy, neurons showed thin spine formation. These inconsistencies may be attributable to interactions between PSD-Zip70 or SPAR and other proteins in addition to the PSD-Zip70 and SPAR interaction. Indeed, Pak et al. (2001) originally reported SPAR as a PSD-95-binding protein and its interaction with actin filaments Rap1 and Snk. Because the amounts of PSD-Zip70 and PSD-95 are believed to be much larger than that of SPAR, PSD-Zip70 may also interact with other proteins and be involved in additional functions in spine morphology. Additional study will be required to elucidate the molecular mechanisms underlying PSD-Zip70-linked spine dynamics.

References

Abe K, Chisaka O, Roy F, Takeichi M (2004) Stability of dendritic spines and synaptic contacts is controlled by α N-catenin. Nat Neurosci 7:357–363.

Bonhoeffer T, Yuste R (2002) Spine motility: phenomenology, mechanisms, and function. Neuron 35:1019–1027.

Carlo S, Piëch V, Wilson NR, Passafaro M, Liu G, Sheng M (2001) Regulation of dendritic spine morphology and synaptic function by shank and homer. Neuron 31:115–130.

Ehlers MD (2003) Activity level controls postsynaptic composition and signaling via the ubiquitin-proteasome system. Nat Neurosci 6:231–242.

El-Husseini AE, Schnell E, Chetkovih DM, Nicoll RA, Bredt DS (2000) PSD-95 involvement in maturation of excitatory synapses. Science 290:1364–1368.

Fischer M, Kaech S, Knutti D, Matus A (1998) Rapid actin-based plasticity in dendritic spines. Neuron 20:847–854.

Goda Y, Davis GW (2003) Mechanisms of synapse assembly and disassembly. Neuron 40:243–264.

Grutzendler J, Kasthurl N, Gan W-B (2002) Long-term dendritic spine stability in the cortex. Nature 420:812–816.

Hayashi K, Shirao T (1999) Change in the shape of dendritic spines caused by overexpression of drebrin in cultured cortical neurons. J Neurosci 19:3918–3925.

Hering H, Shen M (2003) Activity-dependent redistribution and essential role of cortactin in dendritic spine morphogenesis. J Neurosci 23:11759–11769.

Irie F, Yamaguchi Y (2002) EphB receptors regulate dendritic spine development via intersectin, Cdc42 and N-WASP. Nat Neurosci 5:1117–1118.

Ishii H, Vecchione A, Murakumo Y, Baldassarre G, Numata S, Trapasso F, Alder H, Baffa R, Croce CM (2001) FEZ1/LZTS1 gene at 8p22 suppresses cancer cell growth and regulates mitosis. Proc Natl Acad Sci USA 98:10374–10379.

Jontes JD, Smith SJ (2000) Filopodia, spines, and the generation of synaptic diversity. Neuron 27:11–14.

Konno D, Ko JA, Usui S, Hori K, Maruoka H, Inui M, Fujikado T, Tano T, Suzuki T, Tohyama K, Sobue K (2002) The postsynaptic density and dendritic raft localization of PSD-Zip70, which contains an N-myristoylation sequence and leucine-zipper motifs. J Cell Sci 115:4695–4706.

Konno D, Yoshimura S, Hori K, Maruoka H, Sobue K (2005) Involvement of the PI3-kinase/Rac1 and Cdc42 pathways in radial migration of cortical neurons. J Biol Chem, in press.

Lendval B, Stern EA, Chen B, Svoboda K (2000) Experience-dependent plasticity of dendritic spines in the developing rat barrel cortex in vivo. Nature 404:876–881.

Matus A (2000) Actin-based plasticity in dendritic spines. Science 290:754–758.

McGee AW, Bredt DS (2003) Assembly and plasticity of the glutamatergic postsynaptic specialization. Curr Opin Neurobiol 13:111–118.

Meyer G, Brose N (2003) SPARring with spines. Science 302:1341–1344.

Murai KK, Nguyen LN, Irie F, Yamaguchi Y, Pasquale EB (2003) Control of hippocampal dendritic spine morphology through ephrin-A3/EphA4 signaling. Nat Neurosci 6:153–160.

Murase S, Mosser E, Schuman EM (2002) Depolarization drives β-catenin into neuronal spines promoting changes in synaptic structure and function. Neuron 35:91–105.

Okabe S, Urushido T, Konno D, Okado H, Sobue K (2001) Rapid redistribution of the postsynaptic density protein PSD-Zip45 (Homer 1c) and its differential regulation by NMDA receptors and calcium channels. J Neurosci 21:9561–9571.

Pak DTS, Sheng M (2003) Targeted protein degradation and synapse remodeling by an inducible protein kinase. Science 302:1368–1373.

Pak DTS, Yang S, Rudolph-Correia S, Kim E, Sheng M (2001) Regulation of dendritic spine morphology by SPAR, a PSD-95-associated RapGAP. Neuron 31:289–303.

Penzes P, Johnson RC, Sattler R, Zhang X, Huganir RL, Kambampati V, Mains RE, Eipper BA (2001) The neuronal Rho-GEF Kalirin-7 interacts with PDZ domain-containing proteins and regulates dendritic morphogenesis. Neuron 29:229–242.

Penzes P, Beeser A, Chernoff J, Schiller MR, Eipper BA, Mains RE, Huganir RL (2003) Rapid induction of dendritic spine morphogenesis by trans-synaptic ephrinB-EphB receptor activation of the Rho-GEF Kalinrin. Neuron 37:263–274.

Segal M (2001) Rapid plasticity of dendritic spine: hints to possible functions? Prog Neurobiol 63:61–70.

Sheng M, Kim MJ (2002) Postsynaptic signaling and plasticity mechanisms. Science 298:776–780.

Sun J, Tadokoro S, Imanaka T, Murakamk SD, Nakamura M, Kashiwada K, Ko JA, Nishida W, Sobue K (1998) Isolation of PSD-Zip45, a novel Homer/vesl family protein containing leucine zipper motifs, from rat brain. FEBS Lett 437:304–308.

Tachibana T, Imanaka T, Ko JA, Tadokoro S, Nishida W, Sobue K (1999) Isolation of PSD-Zip70, A novel protein containing leucine zipper motif. Cell Struct Funct 24:582.

Tadokoro S, Tachibana T, Imanaka T, Nishida W, Sobue K (1999) Involvement of unique leucine-zipper motif of PSD-Zip45 (Homer 1c/vesl-1L) in group 1 metabotropic glutamate receptor clustering. Proc Natl Acad Sci USA 96:13801–13806.

Tashiro A, Minden A, Yuste R (2000) Regulation of dendritic spine morphology by the rho family of small GTPases: antagonistic roles of Rac and Rho. Cereb Cortex 10:927–938.

Usui S, Konno D, Hori K, Maruoka H, Okabe S, Fujikado T, Tano Y, Sobue K (2003) Synaptic targeting of PSD-Zip45 (Homer 1c) and its involvement in the synaptic accumulation of F-actin. J Biol Chem 278:10619–10626.